Mineralogical Magazine, February 2012, Vol. 76(1), pp. 129–142

The deformation mechanism of a pressure-induced phase transition in dehydrated analcime

A. Yu. Likhacheva[1,*], S. V. Rashchenko[1,2] and Yu. V. Seryotkin[1,2]

[1] Institute of Geology and Mineralogy SibD RAS, pr. ak. Koptyuga 3, 630090 Novosibirsk, Russia
[2] Novosibirsk State University, Pirogov st. 2, 630090 Novosibirsk, Russia

[*Received 8 September 2011; Accepted 19 December 2011; Associate Editor: Wilson Crichton*]

ABSTRACT

The elastic and structural behaviour of dehydrated analcime in compression in a non-penetrating medium up to 3 GPa was studied in a diamond anvil cell using *in situ* synchrotron powder diffraction. A first-order phase transition at 0.4−0.7 GPa is accompanied by a symmetry change from monoclinic (*I*2/*a*) to pseudo-rhombohedral (*R*3) due to trigonalization of the aluminosilicate framework. This is due to the migration of cations to new positions close to the 6-membered rings forming the channels. The reduction of the mean aperture of the structure-forming 6- and 8-membered rings, as a result of tetrahedral tilting, leads to a 7.5% reduction in volume at the phase transition. The bulk modulus values are 38(2) GPa for the low pressure (L*P*) phase [fitted with a Murnaghan equation of state, $K' = 4$ (fixed)] and 11(4) GPa for the high pressure (H*P*) phase [fitted with a third-order Birch−Murnaghan equation of state, $K' = 9(1)$]. The elastic behaviour of the L*P* phase is anisotropic, with compressibilities β_a:β_b:β_c in the ratio 1:4:2; the most compressible direction *b* coinciding with the orientation of empty 8-membered rings. The compressibility of the H*P* phase is isotropic. Trigonalization appears to be the most effective (and probably unique) mechanism of radical volume contraction for the ANA structure type.

Keywords: dehydrated analcime, high pressure, phase transition, compressibility, crystal structure.

Introduction

Analcime, $Na[AlSi_2O_6]\cdot H_2O$, is a widespread mineral, which is defined both as a feldspathoid and a zeolite. One of its characteristic properties is its ability to remain crystalline in a dehydrated form (produced by heating at 550ºC for 0.5 h) for extended periods at ambient conditions (Miroshnichenko and Goryainov, 2000). This behaviour, which is unusual for a zeolite-group mineral, is the result of a significant contraction of the framework, preventing re-absorption of water molecules. The analcime framework (ANA topological type) is built up of 4- and 6-membered tetrahedral rings (4mR and 6mR), which are connected to form 8-membered rings (8mR) (Baerlocher *et al.*, 2001). The 6mRs form regular channels along the [111] direction of the cubic lattice. The highest symmetry ($Ia\bar{3}d$) of the ANA framework topology (Taylor, 1930; Ferraris *et al.*, 1972; Baerlocher *et al.*, 2001) is commonly lowered in natural samples (Mazzi and Galli, 1978; Hazen and Finger, 1979; Pechar, 1988). In cubic analcime the Na sites are two-thirds occupied due to a statistical Si/Al distribution in the framework. The Na sites lying near the centre of 8mRs are six-coordinated by four framework oxygen atoms and two H_2O molecules located in large cages. In dehydrated analcime studied at ambient temperature, an anisotropic contraction of the framework is produced by the migration and concentration of Na cations into new M-positions (within the 8mRs) with unique four-fold planar coordination (Bakakin *et al.*, 1994).

* E-mail: alih@igm.nsc.ru
DOI: 10.1180/minmag.2012.076.1.129

Structural and spectroscopic studies reveal a considerable difference in the high-pressure behaviour of natural (hydrous) and dehydrated analcime (Miroshnichenko and Goryainov, 2000; Gatta *et al.*, 2006). Pressure-induced high-symmetry to low-symmetry displacive phase transitions are observed in natural analcime and isotypic minerals (leucite, pollucite and wairakite) in the pressure range 0.5−2.5 GPa (Gatta *et al.*, 2006, 2008, 2009*a*,*b*). Natural analcime undergoes a phase transition from cubic to triclinic symmetry at about 1 GPa (Gatta *et al*., 2006). This transition is associated with a relatively moderate distortion of the framework resulting in changes in the 8mR and 6mR channel ellipticity and an increase in coordination number of some of the Na atoms to seven. High-pressure Raman spectroscopy shows that dehydrated analcime (DA) has phase transitions at about 0.4 and 1.1 GPa (Miroshnichenko and Goryainov, 2000). The transformation of the Raman doublet at 500 cm^{-1} into a singlet at ~0.4 GPa suggests an increase in effective symmetry (see Miroshnichenko and Goryainov, 2000), which is unusual for high-pressure transformations. In contrast, the transition at 1.1 GPa is associated with substantial loss of symmetry, as indicated by the transformation of the singlet into a triplet. It should be noted that, according to spectroscopic data, the phase transition in natural analcime (NA) at ~1 GPa is accompanied by only minor (<3cm^{-1}) discontinuities in the positions of Raman bands (Goryainov *et al.*, 2000).

These data indicate that the structural changes in dehydrated analcime are more dramatic than in natural hydrous analcime. This difference appears to be related to the absence of non-framework species (H_2O molecules) in W positions in large cages in DA. These molecules prevent significant distortion of the structure. Since there is no structural data on the high-pressure behaviour of DA, this work is devoted to the description of its elastic and structural behaviour during the transition at 0.4 GPa, based on *in situ* synchrotron powder-diffraction data.

Experimental

The sample of analcime used in this study is from the Nidym River, East Siberia, Russia. It has a chemical formula $Na_{1.88}[Al_{1.88}Si_{4.12}O_{12}]\cdot 2H_2O$ (determined by X-ray fluorescence analysis) and is orthorhombic, space group *Ibca*. The powdered sample was heated in a vacuum furnace at 500ºC for 1 h and cooled under vacuum to prevent re-absorption of water. The sample was subsequently kept in a desiccator with calcined silica gel. Even so, the sample still contained 1.9 wt.% water (determined by thermogravimetry), which corresponds to ~25% hydrous analcime. This level of hydration, which was reproduced in several repeated experiments, appears to show the impossibility of keeping analcime fully dehydrated at room temperature and pressure. Indeed, it is well known that 100% dehydration in a zeolite-group mineral can only be maintained at high temperatures, and analcime is no exception. We should note that in previous structural and spectroscopic studies of dehydrated analcime (Bakakin *et al.*, 1994; Goryainov *et al.*, 2000), no data on H_2O content were reported, but the authors did not exclude the presence of water in their samples. It appears that ~2 wt.% water is needed to stabilize dehydrated analcime. Therefore, a NA water-containing orthorhombic phase was included in all of the structural refinements. As the phase transition of NA to the triclinic phase occurs at P >0.9 GPa (Gatta *et al.*, 2006), the refinement of the HP DA structure at 0.9 GPa was performed using orthorhombic NA as a second phase. The unit-cell parameters of DA at ambient pressure and temperature, determined by Rietveld refinement, are a = 13.7249(20), b = 13.5270(14), c = 13.6938(17) Å, β = 90.18(4)º, V = 2542.3(5) $Å^3$, space group *I*2/*a*.

The DA sample was mixed with methanol–ethanol (4:1) and placed in a 400 × 100 μm gasket hole in a diamond anvil cell (DAC) and compressed to 3 GPa. The pressure values were measured using the R1 ruby fluorescence line (Mao *et al.*, 1986) with an accuracy of ~0.05 GPa. The powder diffraction experiments were performed at the 4th beamline of the VEPP-3 storage ring of the SSRC Synchrotron Centre, Novosibirsk (Ancharov *et al.*, 2001), using an X-ray wavelength of 0.3685 Å. A MAR345 imaging plate detector (pixel dimension 100 μm) was used to collect the data. The *FIT2D* program (Hammersley *et al.*, 1996) was used to integrate the two-dimensional images to a maximum 2θ value of 25º. The lattice parameters of DA at different pressures were refined by whole-pattern fitting using the Rietveld method (*GSAS* package; Larson and Von Dreele, 2000). The diffraction profiles collected at ambient pressure (hereafter 0 GPa) and 0.9 GPa were used for the structure refinements.

Rietveld refinement of the crystal structure was performed using data in the 2θ range 2–25º (Table 1). Bragg peak profiles were fitted using a pseudo-Voigt function corrected for asymmetry. Scattering factors for silicon and sodium atoms were used to model the framework (Si,Al) and extraframework Na sites, respectively. The (Si,Al)–O distances for T sites with mixed occupancy were restrained to 1.60(2)–1.67(2) Å, the refined mean values being 1.64 Å for the L*P* phase and 1.62 Å for the H*P* phase, respectively. Due to the complexity of the refined structures, the displacement parameters for all atoms were fixed at an isotropic value of 0.025 $Å^2$ and not refined. The crystal structure of dehydrated analcime (Bakakin *et al.*, 1994) was used as the starting model for the refinement of the L*P* structure at 0 GPa. A structural model in space group *R*3, as proposed for dehydrated (K,Na)-bearing analcime (Seryotkin and Bakakin, 2008), was used for the H*P* structure. Different combinations of the positions of the extraframework species were tried, and the final configuration was chosen on the basis of difference Fourier syntheses, crystal-chemical consistency and the best agreement factors. At the final stages of the refinement, the framework atom coordinates and the coordinates and occupancy factors for the non-framework sites were refined in alternate cycles.

Results and discussion

Elastic behaviour

A comparison of the diffraction patterns of L*P* and H*P* DA (Fig. 1) shows that there is a symmetry change associated with the transition at ~0.4 GPa. The profile of the H*P* phase is similar to dehydrated (K,Na)-bearing analcime, which is stable at ambient pressure with a structure in space group *R*3 (Seryotkin and Bakakin, 2008). Subsequent structure refinement confirmed the choice of space group *R*3 to be appropriate (Fig. 2). Inspection of Fig. 1 shows that the profile shape does not change significantly with increasing pressure above the transition at 0.4 GPa. Therefore, the DA lattice parameters (Fig. 3) at P >0.6 GPa were calculated in space group *R*3. To facilitate comparison with the L*P* structure, the trigonal parameters were transformed to the pseudo-cubic metric of the L*P* phase (Table 2; Fig. 3*a*,*b*). The *c*-axis length in the H*P* trigonal unit cell, 11.6 Å, is half of the length of the volume diagonal in the pseudo-cubic unit cell.

In the pressure range between 0 and 0.6 GPa, the compression of the L*P* DA structure is anisotropic (Fig. 3*a*). The mean axial compressibilities estimated from linear regressions are $\beta_a = 3(3) \times 10^{-3}$, $\beta_b = 1.3(4) \times 10^{-2}$, $\beta_c = 7(2) \times 10^{-3}$ GPa^{-1}. The most compressible direction *b* coincides with the

TABLE 1. Basic crystallographic and experimental data for dehydrated analcime.

Pressure (GPa)	0	0.9
a (Å)	13.7249(20)	18.468(2)
b (Å)	13.5270(14)	18.468(2)
c (Å)	13.6938(17)	11.601(3)
α	90º	90º
β	90.18(4)º	90º
γ	90º	120º
V ($Å^3$)	2542.3(5)	3426.5(8)
Space group	*I*2/*a*	*R*3
Radiation	λ = 0.3685 Å	
2θ range (º)	2–25	2–25
Number of observations	2441	2440
Number of variables	51	91
Number of reflections	3040	2202
R_p	0.011	0.006
R_{wp}	0.017	0.009
R_{F2}	0.12	0.13
χ^2	0.32	2.5

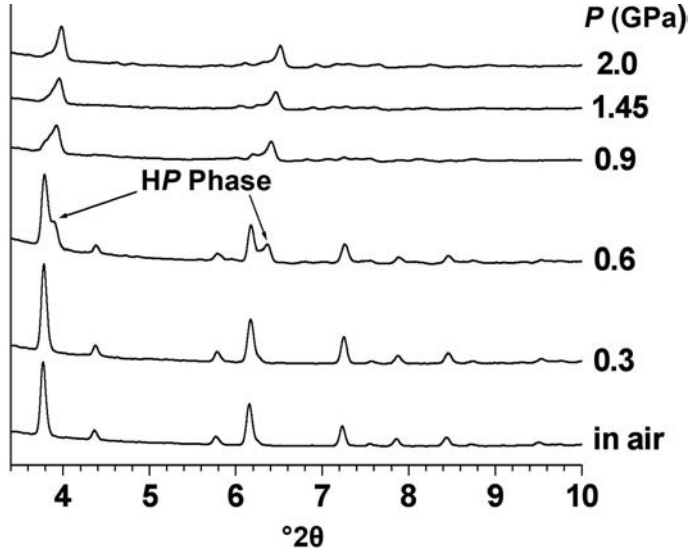

FIG. 1. Powder diffraction traces for dehydrated analcime at different pressures. At 0.6 GPa both the L*P* and H*P* phase (marked by arrows) are present in the sample. The diffraction data are plotted to 10º2θ to give a detailed picture of the changes associated with the transition to the H*P* phase.

orientation of empty 8mRs; two-thirds of the 8mRs oriented along *a* and *c* are filled with Na^+ cations (Bakakin *et al.*, 1994).

The ~7.5% volume contraction observed at the phase transition (Fig. 3*b*) is comparable to or slightly greater than the maximum volume discontinuities observed for the ANA structure type [during dehydration of (Li,Na)-bearing and (K,Na)-bearing analcime (Seryotkin *et al.*, 2005; Seryotkin and Bakakin, 2008)]. It is noteworthy that both of these types of analcime undergo the same type of deformation (trigonalization) during dehydration. However, the volume change produced by the phase transition in natural analcime at ~1 GPa (Gatta *et al.*, 2006) is only 1.9%. This shows that there is a significant difference in the H*P* deformation mechanisms in DA and NA.

TABLE 2. Lattice parameters for dehydrated analcime at different pressures.

P (GPa)	*a* (Å)	*b* (Å)	*c* (Å)	β (º)		*V* (Å^3)
	L*P* phase (space group *I*2/*a*)					
0	13.7249(20)	13.5270(14)	13.6938(17)	90.18(4)		2542.3(5)
0.3	13.6864(29)	13.4974(22)	13.6474(32)	90.07(9)		2521.1(7)
0.6	13.698(13)	13.418(6)	13.634(8)	90.17(26)		2505.8(26)
	H*P* phase					
	Trigonal (space group *R*3)			Pseudo-cubic		
	a (Å)	*c* (Å)	*V* (Å^3)	*a* (Å)	α (º)	*V* (Å^3)
0.6	18.592(9)	11.599(12)	3472.1(34)	13.229	89.29	2314.6
0.9	18.4727(22)	11.5955(24)	3426.7(7)	13.172	89.05	2284.3
0.97	18.4442(19)	11.5777(20)	3410.9(7)	13.152	89.05	2273.7
1.45	18.2974(18)	11.4571(20)	3321.9(7)	13.036	89.15	2214.4
2.0	18.1866(18)	11.3177(22)	3241.8(7)	12.930	89.39	2161.0
3.17	17.9919(29)	11.1882(27)	3136.5(11)	12.788	89.42	2090.8

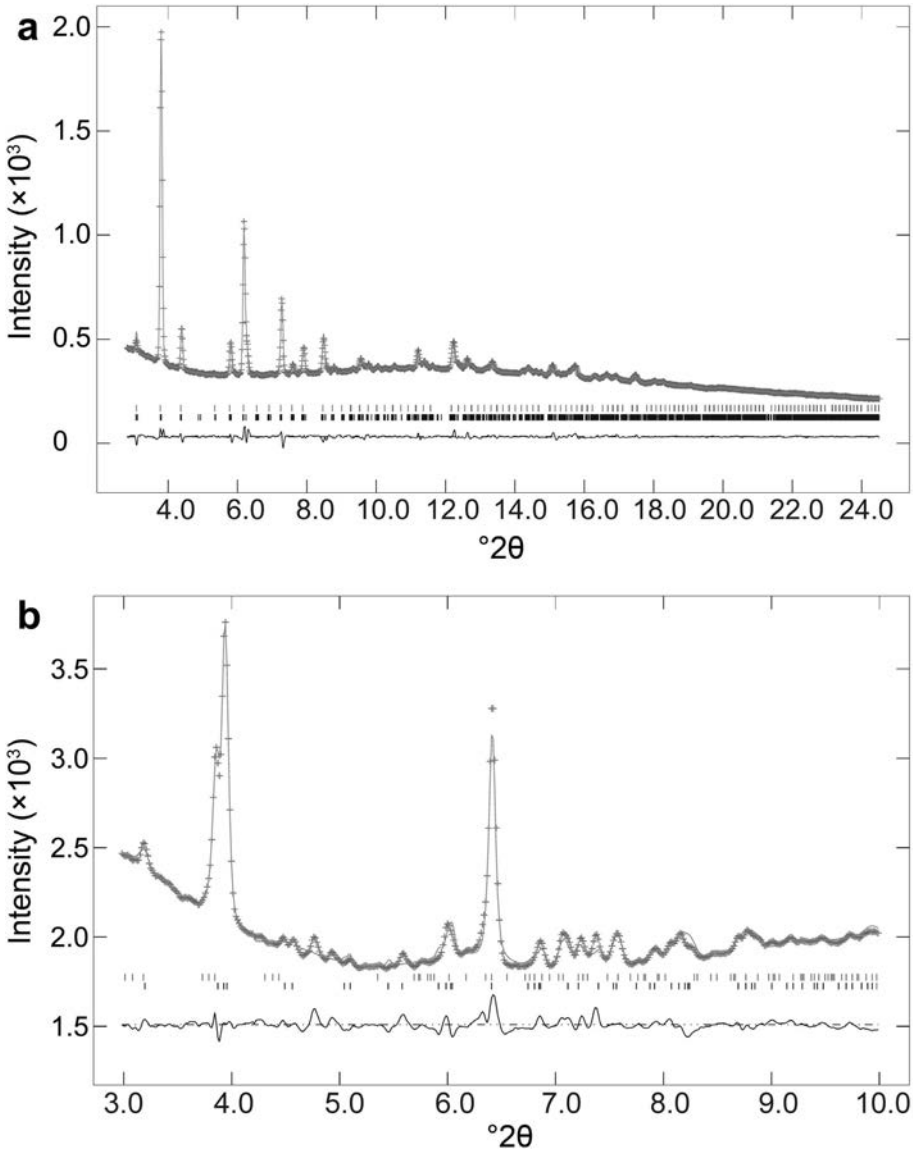

FIG. 2. Rietveld refinements of DA at (*a*) 0 GPa and (*b*) 0.9 GPa. The observed and calculated profiles are indicated by the + symbol and a continuous line, respectively. Tick marks indicate the positions of Bragg peaks that are allowed in orthorhombic natural analcime (upper) and monoclinic L*P* (*a*) and trigonal H*P* (*b*) DA phases (lower). A difference curve is plotted at the bottom.

Figures 1 and 3*b* show that neither the profile shape nor the volume compressibility of DA have appreciable variations in the pressure range between 0.9 and 3 GPa, which implies that less dramatic structural changes are associated with the second phase transition at ~1.1 GPa (Miroshnichenko and Goryainov, 2000). Therefore, $P-V$ data in the pressure range 0.9−3 GPa were used as a whole to obtain the elastic parameters. Fitting the volume data of the monoclinic (L*P*) phase using the Murnaghan equation of state (Murnaghan, 1937) gives V_0 = 2542.29(5) Å^3, K_0 = 38(2) GPa, K' = 4 (fixed); Fig. 3*b*. Fitting the volume data of the trigonal

(re-calculated to the cubic metric) H*P* phase (Table 2) using the third-order Birch–Murnaghan equation of state (Angel, 2001) gives V_0 = 2430(15) Å^3, K_0 = 11(4) GPa, K' = 9(1); Fig. 3*b*. The bulk modulus, K_0, of the L*P* phase is comparable with the mean K_0 value for natural zeolites (Gatta, 2008) but is appreciably less than the bulk modulus of L*P* natural analcime (56(3) GPa; Gatta *et al.*, 2006). An abrupt increase of the DA compressibility upon the phase transition is similar with that observed in the NA H*P* phase (Gatta *et al.*, 2006) but is even larger, this appears to be related to incomplete filling of the framework cavities.

The axial compressibilities of the H*P* DA structure estimated using linear regression are $\beta_{a(\mathrm{trig})} = 1.2(1)\times10^{-2}$ and $\beta_{c(\mathrm{trig})} = 1.5(1)\times10^{-2}$ GPa^{-1} for the trigonal metric (Fig. 3*c*) and $\beta_{a(\mathrm{cub})} = 1.3(1)\times10^{-2}$ GPa^{-1} for the cubic metric (Fig. 3*a*), showing that compression is almost isotropic in the pressure range 0.8–3 GPa.

The structure of high-pressure dehydrated analcime at 0.9 GPa

The results of Rietveld refinement of the L*P* and H*P* DA structures are shown in Fig. 2, atom coordinates are listed in Tables 3 and 4, and selected structural parameters for the framework bonds and cation environment are given in Tables 5 and 6, respectively. In the DA structure at 0 GPa all the framework distances and angles, as well as the distances in the cation polyhedra, are in reasonable agreement with previous single-crystal data (Bakakin *et al.*, 1994). The refined L*P* and H*P* structures are drawn, for ease of comparison, perpendicular to the 6mR channel in Fig. 4. As noted above, the *c* axis of the unit-cell in the H*P* phase, 11.6 Å, is half of the length of the volume diagonal in the pseudo-cubic unit cell. It corresponds to the framework channel formed by 6mRs and contains two large cavities (Fig. 5). It should be noted that one low-intensity diffraction peak at 4.7°2θ cannot be accounted for in the refinements in space group *R*3 (Fig. 2*b*), indicating that the real symmetry of the H*P*

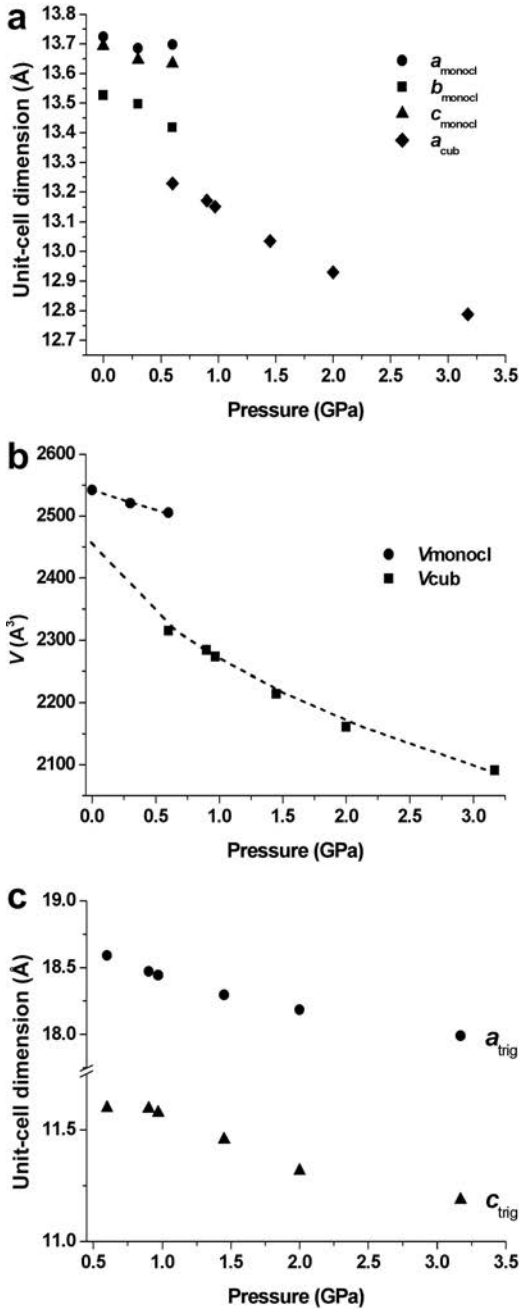

FIG. 3. Pressure dependence of the lattice parameters and unit-cell volume of dehydrated analcime. (*a*) Pressure dependence of the lattice parameters of monoclinic L*P* DA below the phase transition and of H*P* DA (on the basis of a pseudo-cubic unit cell) above the phase transition. (*b*) Pressure dependence of the volume of the unit cell in DA above and below the phase transition with fits to the equations of state shown as dashed lines. (*c*) Pressure dependence of the trigonal unit-cell parameters in DA above the phase transition.

TABLE 3. Atom coordinates for dehydrated analcime at ambient pressure.

Atom	*x*/*a*	*y*/*b*	*z*/*c*
T11A	0.1219(11)	0.1594(11)	0.4098(10)
T11B	0.8770(11)	0.3402(11)	0.4086(10)
T12A	0.4189(11)	0.1246(11)	0.1677(11)
T12B	0.5816(11)	0.3759(11)	0.1685(11)
T2A	0.1598(5)	0.4093(6)	0.1289(6)
T2B	0.8410(5)	0.0905(6)	0.1277(6)
O11A	0.0982(5)	0.3527(6)	0.2165(4)
O11B	0.9033(5)	0.1466(6)	0.2151(4)
O12A	0.3865(6)	0.1362(6)	0.47170(33)
O12B	0.6132(6)	0.3632(6)	0.47316(33)
O21A	0.22360(32)	0.1138(6)	0.3617(7)
O21B	0.77564(32)	0.3868(6)	0.3610(7)
O22A	0.1461(5)	0.47037(34)	0.3647(7)
O22B	0.8523(5)	0.02977(34)	0.3620(7)
O31A	0.3882(7)	0.2187(4)	0.1018(5)
O31B	0.6140(7)	0.2812(4)	0.1040(5)
O32A	0.4661(4)	0.3992(6)	0.1524(6)
O32B	0.5346(4)	0.1016(6)	0.1537(6)
M11	0.1533(30)	0.9820(35)	0.2791(23)
M2	0.006(6)	0.259(5)	0.1040(23)

TABLE 4. Atom coordinates for dehydrated analcime at 0.9 GPa (space group *R*3).

Atom	*x*/*a*	*y*/*b*	*z*/*c*	Occupancy
T1	0.1788(5)	0.0786(5)	0.5450(8)	1.0
T2	0.3326(5)	0.1921(5)	0.4085(8)	1.0
T3	0.4927(5)	0.2208(5)	0.2843(8)	1.0
T4	0.4517(5)	0.1280(5)	0.0828(8)	1.0
T5	−0.1796(5)	−0.0730(5)	−0.5309(8)	1.0
T6	−0.3405(5)	−0.2022(5)	−0.4199(8)	1.0
T7	−0.4890(5)	−0.2142(5)	−0.3098(8)	1.0
T8	−0.4667(5)	−0.1287(5)	−0.0834(8)	1.0
O1	0.1519(5)	0.1484(5)	0.5568(12)	1.0
O2	0.1870(11)	0.0532(7)	0.6734(8)	1.0
O3	0.2576(6)	0.1053(8)	0.4646(11)	1.0
O4	0.4016(5)	0.1650(7)	0.3556(12)	1.0
O5	0.2906(5)	0.2282(7)	0.3167(11)	1.0
O6	0.4684(12)	0.2058(6)	0.1523(8)	1.0
O7	0.5683(4)	0.2108(8)	0.3275(17)	1.0
O8	0.4456(6)	0.0630(6)	0.1762(9)	1.0
O9	−0.1201(4)	−0.1130(7)	−0.5113(15)	1.0
O10	−0.1737(14)	−0.0528(8)	−0.6642(7)	1.0
O11	−0.2794(5)	−0.1328(10)	−0.5123(12)	1.0
O12	−0.3906(5)	−0.1723(8)	−0.3364(13)	1.0
O13	−0.2899(6)	−0.2357(7)	−0.3427(10)	1.0
O14	−0.5017(14)	−0.2118(7)	−0.1701(7)	1.0
O15	−0.5264(6)	−0.1667(6)	−0.3747(16)	1.0
O16	−0.4631(7)	−0.0493(6)	−0.1520(9)	1.0
Ow1	0.0	0.0	0.825(21)	0.56(15)
Na11	0.119(24)	0.114(20)	0.754(33)	0.27(5)
Na2	0.0	0.0	0.359(10)	1.01(12)
Na3	0.9289(32)	0.190(4)	0.188(7)	0.97(5)
Na4	0.326(4)	0.363(5)	0.518(7)	0.99(4)

TABLE 5. Selected structural parameters (Å, º) for L*P* and H*P* dehydrated analcime.

L*P* phase at 0 GPa		H*P* phase at 0.9 GPa	
4-ring(1)		4-ring(1)	
O12A–O12A	3.82(4)	O1–O5	3.56(6)
O21A–O21A	3.85(4)	O3–O10	3.65(6)
ε[1]	0.99	ε	0.98
T11A–O21A–T2A	149.5(8)	T1–O1–T5	131.7(9)
T11A–O12A–T2A	150.2(8)	T1–O3–T2	137.1(12)
		T2–O5–T8	143.1(7)
		T5–O10–T8	136.8(17)
4-ring(2)		4-ring(2)	
O22A–O22B ×2	3.20(5)		
O11A–O11B ×2	4.08(5)	O15–O16	3.19(7)
ε	0.78	O4–O14	3.82(6)
T12A–O11A–T2A	133.7(7)	ε	0.84
T12B–O11B–T2B	133.1(7)	T2–O4–T3	131.5(9)
T12A–O22A–T2B	149.4(8)	T7–O14–T8	128.6(8)
T12B–O22B–T2A	149.0(8)	T3–O15–T7	142.0(11)
		T2–O16–T8	157.2(8)
4-ring(3)		4-ring(3)	
O31A–O31B	3.21(5)		
O32A–O32B	4.13(5)	O7–O8	3.07(6)
ε	0.78	O6–O12	4.28(7)
T11A–O31A–T12A	148.9(9)	ε	0.72
T11B–O31B–T12B	149.6(9)	T3–O6–T4	125.3(11)
T11A–O32A–T12B	132.6(8)	T3–O7–T7	151.4(9)
T11B–O32B–T12A	132.5(8)	T4–O8–T6	158.4(9)
		T6–O12–T7	130.8(9)
6-ring(1)		6-ring(1)	
O21A–O21A	4.84(4)	O1–O9 ×3	4.99(6)
O11A–O11A	5.08(4)	ε	1
O31A–O31A	5.62(4)		
ε	0.88	6-ring(2)	
		O7–O15 ×3	4.95(6)
6-ring(2)		ε	1
O21B–O21B	4.84(4)		
O11B–O11B	5.14(4)	6-ring(3)	
O31B–O31B	5.52(4)	O3–O11	4.66(7)
ε	0.90	O8	5.01(6)
		O2	5.08(7)
		ε	0.95
8-ring(1)		8-ring(1)	
O11A–O11B	3.86(5)	O1–O6	3.70(6)
O12A–O12B	4.37(5)	O2–O15	4.23(6)
O31A–O32A	7.77(5)	O2–O12	6.94(6)
O31B–O31B	6.89(4)	O8–O9	6.97(6)
ε	0.56	ε	0.60
8-ring(2)		8-ring(2)	
O22A–O22A	4.66(4)	O9–O14	4.30(6)
O31A–O31A	4.70(4)	O7–O10	4.59(6)
O12A–O12B	7.20(5)	O3–O14	6.34(6)
O21A–O21B	7.39(5)	O5–O15	7.36(6)
ε	0.64	ε	0.65
		6-ring(4)	
		O4–O12	4.74(7)
		O6–O14	5.01(7)
		O5–O13	5.14(7)
		ε	0.95

Table 5 (*contd.*)

—— L*P* phase at 0 GPa ——		—————— H*P* phase at 0.9 GPa ——————			
———— 8-ring(3) ————		— 8-ring(3) —		—— 8-ring(4) ——	
O32A−O32B	3.81(5)	O5−O12	4.02(7)	O10−O14	4.36(7)
O21A−O21B	4.32(5)	O11−O16	4.63(7)	O7−O16	4.44(7)
O11A−O22A	6.95(5)	O5−O16	7.21(6)	O4−O10	6.58(7)
O11A−O22B	7.78(5)	O10−O14	7.77(7)	O1−O16	7.37(7)
ε	0.55	ε	0.58	ε	0.63

[1] The ellipticity values are defined as follows: $\varepsilon_{(4\text{-rings})}$ = (O12A−O12A)/(O21A−O21A); $\varepsilon_{(6\text{-rings})}$ are half of the sum of the two short O−O diagonals divided by the longer one (e.g. (O21A−O21A + O11A−O11A)/2(O31A−O31A)); $\varepsilon_{(8\text{-rings})}$ are the sum of two short O−O diagonals divided by the sum of two long ones (e.g. (O11A−O11B + O12A−O12B)/(O31A−O32A + O31B−O31B)).

structure is lower. However, if the symmetry was lowered further, the solution of the structure would be complicated, or almost unrealizable, with the limited powder-diffraction data available. Therefore, we decided to use a trigonal model for the structure of H*P* DA, although it is only an approximation. The refinement parameters (Table 1) from the trigonal model are sufficiently good to allow us to draw definite conclusions about the structural deformation in the phase transition.

In comparison to the L*P* structure, all the tetrahedral rings (4mR, 6mR, 8mR) are deformed. To quantify the changes produced by the transition, ellipticity ratios, ε, were calculated (Table 5). In the L*P* structure below the transition, all the 6mRs are slightly elliptical (Fig. 4*a*), whereas in the H*P* structure they are perfectly trigonal in the central channel parallel to *c* (Figs 4*b* and 5*b*) and close to trigonal in the 'side' channels, their mean aperture being reduced by ~4%. In the phase transition, the 4mRs 'split' into more and less elliptical geometries and become more twisted. The ellipticity of the 8mR does not change much, but the mean aperture decreases by ~2%. This is a result of cooperative tilting of tetrahedra, which is indicated by increases of the ranges of T−O−T angles inside the rings from 133−150º to 129−157º for 6mRs, 125−158º for 4mRs, and 128−158º for 8mRs.

TABLE 6. Bond distances (Å) around the non-framework cations at 0 and 0.9 GPa.

— L*P* phase at 0 GPa —		—————— H*P* phase at 0.9 GPa ——————			
M11−O21A	2.32(4)	Na11−O1	2.4(4)	Na3−O4	3.00(8)
M11−O21B	2.51(4)	Na11−O2	2.3(5)	Na3−O12	2.70(7)
M11−O32A	2.48(4)	Na11−O6	2.3(6)	Na3−O13	2.99(8)
M11−O32B	2.62(4)	Na11−O15	2.5(4)	Na3−O14	2.41(7)
		Na11−Ow1	2.31(9)		
Average Na−O	2.48	Average Na−O	2.38	Average Na−O	2.78
M2−O11A	2.36(6)	Na2−O9 ×3	2.63(7)	Na4−O5	2.4(7)
M2−O11B	2.57(6)	Na2−O10 ×3	2.86(1)	Na4−O11	2.89(6)
M2−O12A	2.29(7)			Na4−O12	2.83(7)
M2−O12B	2.55(7)			Na4−O16	2.72(8)
Average Na−O	2.44	Average Na−O	2.75	Average Na−O	2.71
		Ow1−O7	2.9(2)	Na11−Na11	3.7(5)
M11−M2	4.05(8)	Ow1−O6	3.2(2)	Na11−Na4	3.6(3)
				Na4−Na4	4.02(4)

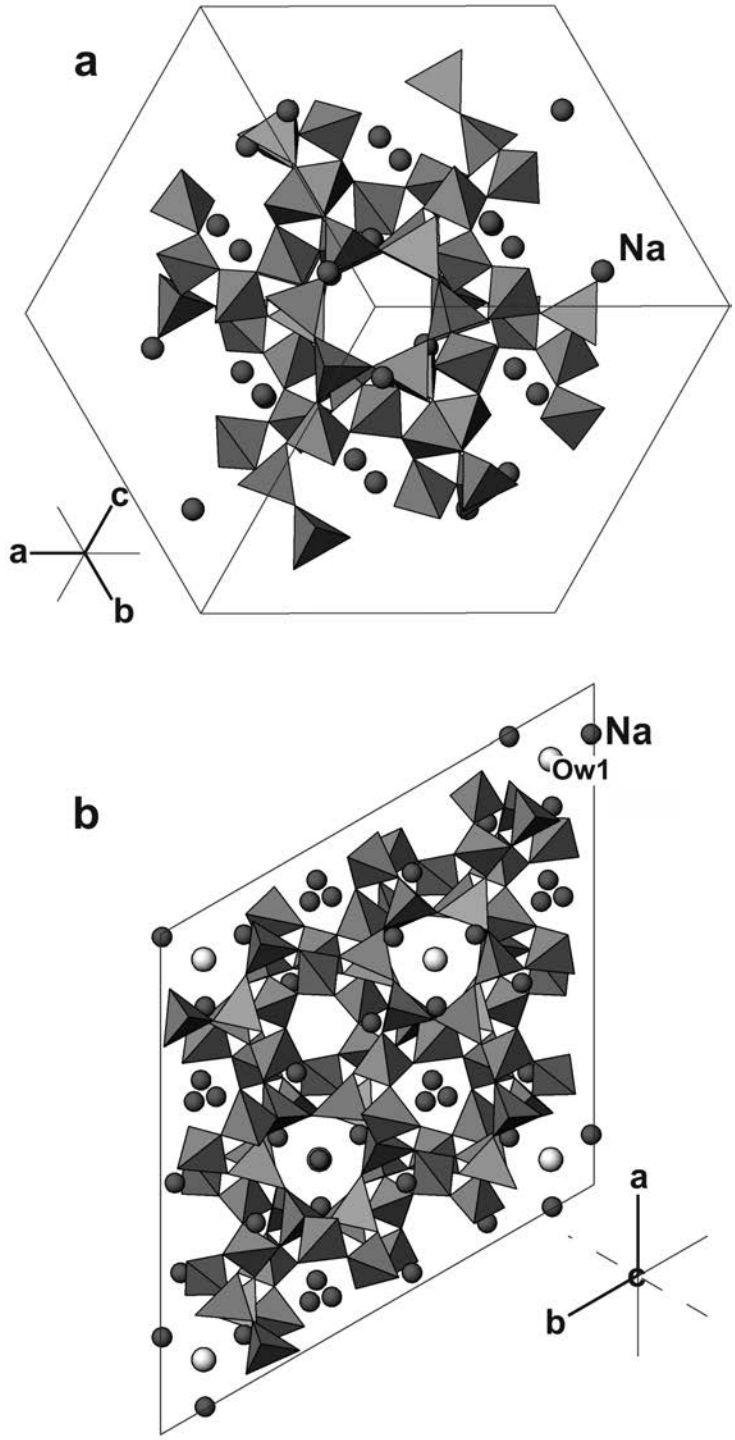

FIG. 4. The crystal structure of dehydrated analcime. (*a*) The L*P* phase at 0 GPa. (*b*) the H*P* phase at 0.9 GPa.

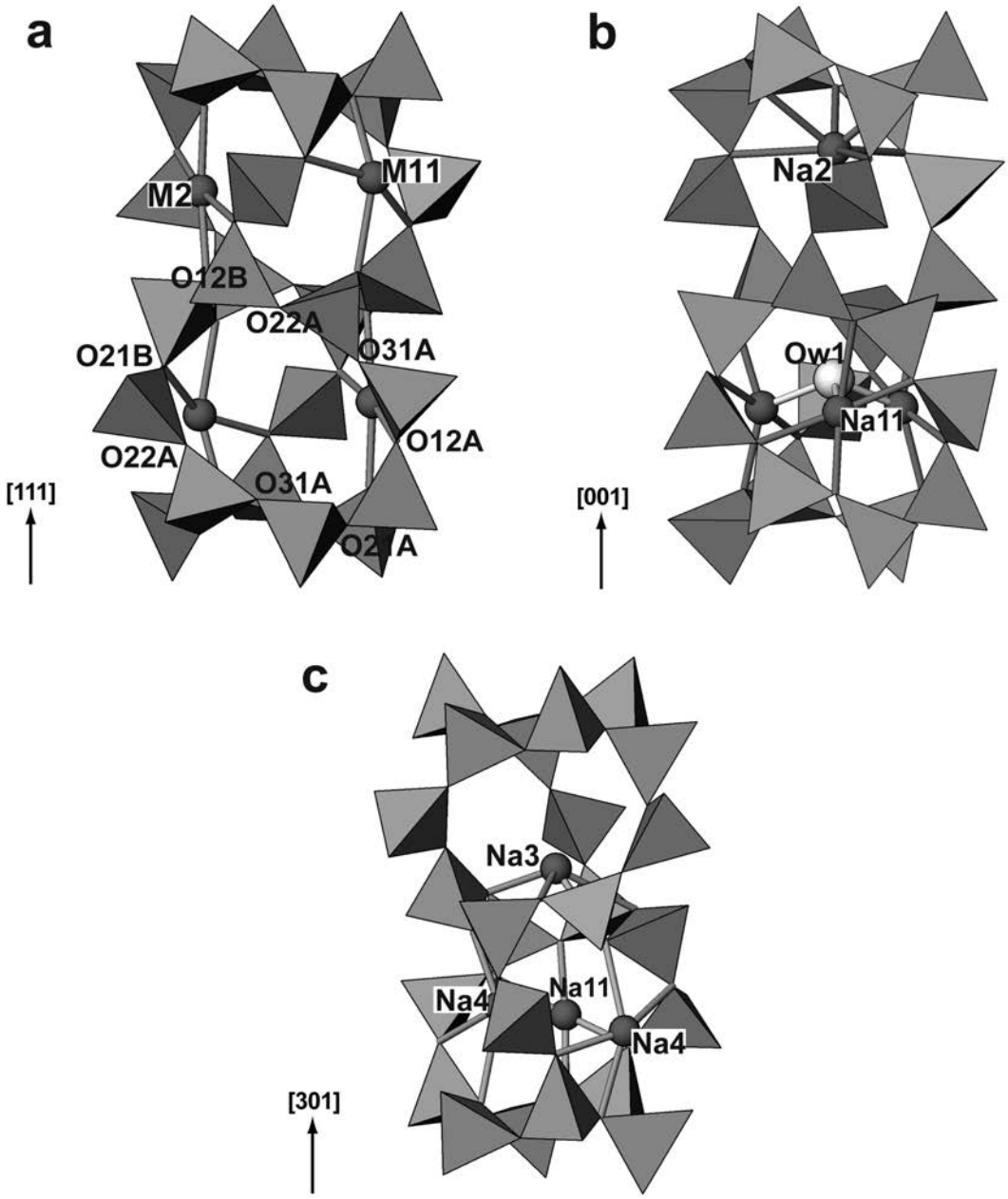

FIG. 5. Local coordination of Na in the channel formed by the 6mRs. (*a*) The LP phase at 0 GPa (*b*) The main three-fold channel in the H*P* phase at 0.9 GPa. The short distances Ow−Na in the H*P* structure (see Table 5) are marked in a lighter shade of grey. (*c*) A 'side' channel in the H*P* phase at 0.9 GPa.

The deformation of the tetrahedral rings leads to a reduction of the isometric cavities and a volume contraction of 7.5%.

The emergence of three-fold symmetry is due to the migration of some cations to new positions close to the 6mRs that form the channels. In the

L*P* structure the Na sites, which occupy two thirds of the 8mRs, are coordinated by four framework O atoms (Figs 4*a* and 5*a*; Table 6). In the H*P* structure, one new position, Na2, lies at the centre of the channel (on the three-fold axis) and is coordinated by six O atoms of the 6mR (Figs 4*b* and 5*b*). The 'side' channel also contains one new Na3 site near to the 6mR, but shifted from the channel centre (Fig. 5*c*) and coordinated by four O atoms of the 6mR. Both of the 'channel' Na positions are characterized by longer mean Na−O distances of about 2.8 Å (Table 6). Two other Na sites lie inside the 8mR, one (Na11) being similar to the M site in the L*P* structure, with planar four-fold coordination and a shortened mean Na−O distance of 2.4 Å. Another Na site, Na4, is slightly shifted from 8mR into the large cage, which results in a larger mean Na−O distance of 2.7 Å and a shortened Na11−Na4 distance of 3.6 Å. In total, half of the cations in the H*P* structure move to new positions in the centre of the channels.

Additional electron density revealed by a difference Fourier synthesis in the three-fold channel in the vicinity of Na11 is interpreted as an H_2O site (Ow1, Fig. 5*b*; Table 6). The refinement of Ow1 occupancy (Table 4) gives an H_2O content of 0.08 *per* 1 Na. We suppose that such a small quantity of water could not be located in the L*P* structure due to its statistical distribution in the large cavities. Regardless of whether the water is present in the initial DA or is the result of pressure-induced hydration (small amounts of water could be present in the methanol−ethanol medium), it does not influence the H*P* behaviour of DA strongly. The phase transition in DA differs fundamentally from the transition in NA.

The different behaviour of cations in the pressure-induced phase transitions results in different types of framework distortion in the DA and NA structures. The high mobility of the non-framework cations in DA is caused by the presence of large empty cavities, which appear to be the most unstable elements of the structure as the pressure is increased. Partial filling of these cavities by cations in the H*P* DA structure provides support for the framework and reduces the volume. The 6mRs undergo the largest deformation (trigonalization) due to the appearance of nearby Na sites. The mean Na−O distances increase in the H*P* DA structure due to the shift of Na cations into the large cages; by contrast, in the H*P* NA structure the mean Na−O distances decrease as a result of contraction of the 8mR accommodating the cations (Gatta *et al.*, 2006).

The structural changes described above in H*P* DA are similar to those that occur when (Li,Na)-bearing analcime and (K,Na)-bearing analcime dehydrate at ambient pressure (Seryotkin *et al.*, 2005; Seryotkin and Bakakin, 2008). In both of these compounds, removal of H_2O molecules from the W sites in large cages allows the migration of some cations into new positions close to 6mRs and trigonalization of the structure. The variability in T−O−T angles in dehydrated (Li,Na)-analcime (121.3−158.9º) is even larger than in the H*P* DA structure.

We should note that the twisting of 4mR upon the phase transition leads to a better uniformity of their mean T−O−T angles, as compared to the L*P* DA structure (Table 5). Along with the increase of apparent symmetry revealed by the diffraction data, this agrees with the Raman spectroscopy observations (Miroshnichenko and Goryainov, 2000) showing the transformation of the strong Raman doublet at ~500 cm^{-1} to a singlet, this band being assigned to the vibrations in 4mR.

Conclusions

In situ synchrotron powder diffraction data show that a first-order phase transition observed at 0.4−0.7 GPa in dehydrated analcime is accompanied by a symmetry change from monoclinic (*I*2/*a*) to pseudo-rhombohedral (*R*3). This is an unusual case of a pressure-induced increase in the symmetry in a silicate mineral. The structural model proposed for the H*P* phase seems to give a reasonable explanation of the observed trigonalization. It is due to the migration of half of the Na cations into new positions close to the 6-membered rings forming the channels. As a result, these rings become trigonal. The high mobility of the non-framework cations in dehydrated analcime is caused by the presence of large empty cavities which are unstable with respect to compression. Partial filling of these cavities by Na cations in the H*P* structure provides support for the framework. The decrease of mean apertures of the structure-forming 6-membered and 8-membered rings through tetrahedral tilting leads to a 7.5% reduction in volume, which is the maximum volume discontinuity observed for the ANA structure type to date.

The elastic behaviour of the L*P* dehydrated analcime is anisotropic, the most compressible

direction *b* coinciding with the orientation of empty 8-membered rings. The H*P* DA structure is isotropic in compression. The bulk modulus of the L*P* phase, 38(2) GPa, is comparable with the mean bulk modulus for zeolite-group minerals, but appreciably smaller than the value for L*P* natural analcime (Gatta *et al.*, 2006). The large increase in the compressibility of DA above the phase transition, K_0 = 11(4) GPa, is similar to that observed in natural analcime (Gatta *et al.*, 2006).

The deformation mechanism of the H*P* phase transition in dehydrated analcime is similar to that found in the dehydration of (Li,Na)-bearing analcime and (K,Na)-bearing analcime at ambient pressures. Trigonalization appears to be the most effective (and probably unique) mechanism of radical volume contraction for the ANA structure type.

Acknowledgements

We thank Dr S.V. Goryainov for valuable discussions. The study was carried out using the equipment belonging to the Novosibirsk SCSTR Synchrotron centre (Russia) and within the framework of State Contract No. 16.552.11.7044. This work is supported by RFBR grant 11-05-01121.

References

Ancharov, A.I., Manakov, A.Yu., Mezentsev, N.A., Tolochko, B.P., Sheromov, M.A. and Tsukanov, V.M. (2001) New station at the 4th beamline of the VEPP-3 storage ring. *Nuclear Instruments and Methods of Physical Research A*, **470**, 80–83.

Angel, R.I. (2001) *EOS-FIT V6.0 Computer program*. Crystallography Laboratory, Department of Geological Sciences, Virginia Tech, Blacksburg, USA.

Baerlocher, Ch., Meier, W.M. and Olson, D.H. (2001) *Atlas of zeolite framework types*, fifth edition. Elsevier, Amsterdam, 302 pp.

Bakakin, V.V., Alekseev, V.I., Seryotkin, Yu.V., Belitsky, I.A., Fursenko, B.A. and Balko, V.P. (1994) Crystal structure of dehydrated analcime. Plane 4-fold coordination of sodium. *Doklady Akademii Nauk*, **339**, 520–524.

Ferraris, G., Jones, D.W. and Yerkess, J. (1972) A neutron-diffraction study of the crystal structure of analcime, $NaAlSi_2O_6 \cdot H_2O$. *Zeitschrift für Kristallographie*, **135**, 240–252.

Gatta, G.D. (2008) Does porous mean soft? On the elastic behaviour and structural evolution of zeolites under pressure. *Zeitschrift für Kristallographie*, **223**, 160–170.

Gatta, G.D., Nestola, F. and Ballaran, T.B. (2006) Elastic behavior, phase transition, and pressure induced structural evolution of analcime. *American Mineralogist*, **91**, 568–578.

Gatta, G.D., Rotiroti, N., Boffa Ballaran, T. and Pavese, A. (2008) Leucite at high pressure: elastic behaviour, phase stability and petrological implications. *American Mineralogist*, **93**, 1588–1596.

Gatta, G.D., Rotiroti, N., Boffa Ballaran, T., Sanchez-Valle, C. and Pavese, A. (2009*a*) Elastic behaviour and phase-stability of pollucite, a potential host for nuclear waste. *American Mineralogist*, **94**, 1137–1143.

Gatta, G.D., Sartbaeva A. and Wells, A.S. (2009*b*) Compression behaviour and flexibility window of the analcime-like feldspathoids: experimental and theoretical findings. *European Journal of Mineralogy*, **21**, 571–580.

Goryainov, S.V., Belitsky, I.A., Likhacheva, A.Yu. and Fursenko, B.A. (2000) Raman spectroscopy of high-pressure phase transitions in analcime and leucite. *Russian Geology and Geophysics*, **41**, 673–681.

Hammersley, A.P., Svensson, S.O., Hanfland, M., Fitch, A.N. and Hausermann, D. (1996) Two-dimensional detector software: from real detector to idealized image or two-theta scan. *High-Pressure Research*, **14**, 235–248.

Hazen, R.M. and Finger, L.W. (1979) Polyhedral tilting: a common type of pure displacive phase transition and its relationship to analcime at high pressure. *Phase Transitions*, **1**, 1–22.

Larson, A.C. and Von Dreele, R.B. (2000) *General structure analysis system (GSAS)*. Report LAUR 86-748, Los Alamos National Lab, New Mexico, USA.

Mao, H.K., Xu, J. and Bell, P.M. (1986) Calibration of the ruby pressure gauge to 800 kbar under quasi-hydrostatic conditions. *Journal of Geophysical Research*, **91**, 4673–4676.

Mazzi, F. and Galli, E. (1978) Is each analcime different? *American Mineralogist*, **63**, 448–460.

Miroshnichenko, Y.M. and Goryainov, S.V. (2000) Raman study of high-pressure phase transitions in dehydrated analcime. *Mineralogical Magazine*, **64**, 301–309.

Murnaghan, F.D. (1937) Finite deformations of an elastic solid. *American Journal of Mathematics*, **49**, 235–260.

Pechar, F. (1988) The crystal structure of natural monoclinic analcime ($NaAlSi_2O_6 \cdot H_2O$). *Zeitschrift für Kristallographie*, **184**, 63–69.

Seryotkin, Yu.V. and Bakakin, V.V. (2008) The thermal behavior of secondary analcime and leucite derivate and its structural interpretation. *Russian Geology and Geophysics*, **49**, 207–213.

Seryotkin, Yu.V., Bakakin, V.V. and Bazhan, I.S. (2005) The structure of dehydrated ($Li_{0.7}Na_{0.3}$)-analcime: a

trigonal deformation of the framework and new low-coordinated non-framework positions. *Journal of Structural Chemistry*, **46**, 681–693.

Taylor, W.H. (1930) The structure of analcime ($NaAlSi_2O_6 \cdot H_2O$). *Zeitschrift für Kristallographie*, **74**, 1–19.